Supplementary Materials

Conjugated polycarboxylate ligands-coordinated NiFe LDH for enhanced oxygen evolution

Zi-Ye Liu[a], Qian-Yu Wang[a], Teng Xu[a], Ji-Ming Hu* [a,b]

[a] Department of Chemistry, Zhejiang University, Hangzhou 310058, P. R. China

[b] Southern Marine Science and Engineering Guangdong Laboratory (Zhuhai), Zhuhai 519080, P.R. China

*: Corresponding author. E-mail: kejmhu@zju.edu.cn. Tel: +86-571-87953297. Fax: +86-571-87951895.

Supplementary datas

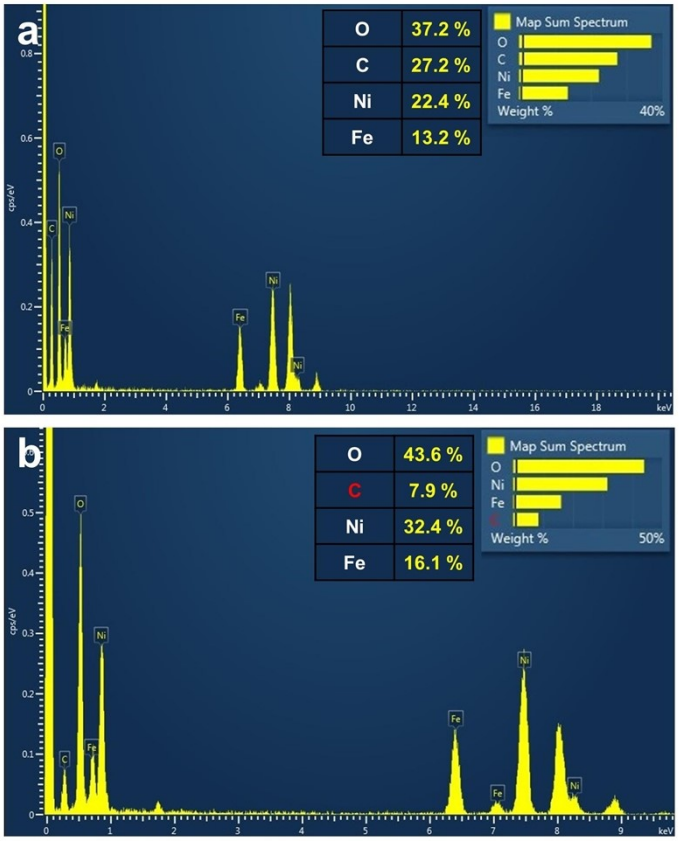

Figure S1. EDS results of (a) cp-OA(40) LDH and (b) cp-Ni_2Fe_1 LDH.

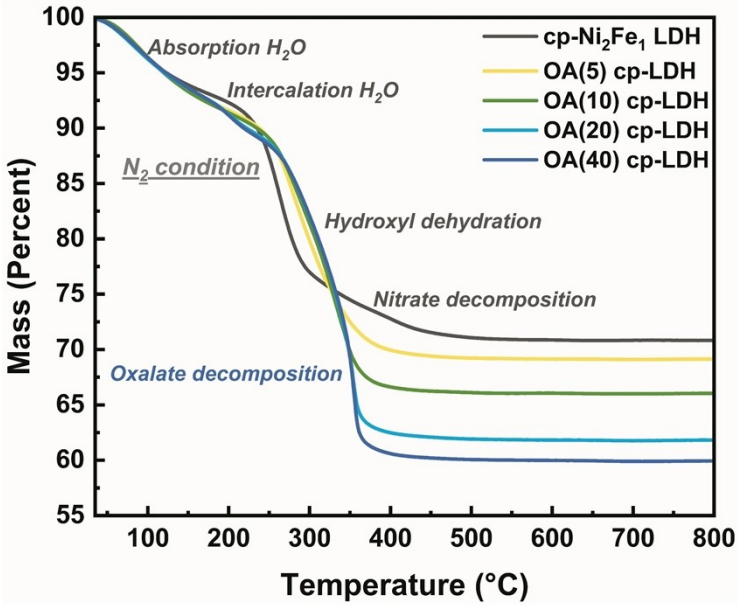

Figure S2. Thermogravimetry analysis of cp-Ni_2Fe_1 LDH and cp-OA(n) NiFe LDH(n= 5, 10, 20, 40) in N_2 condition

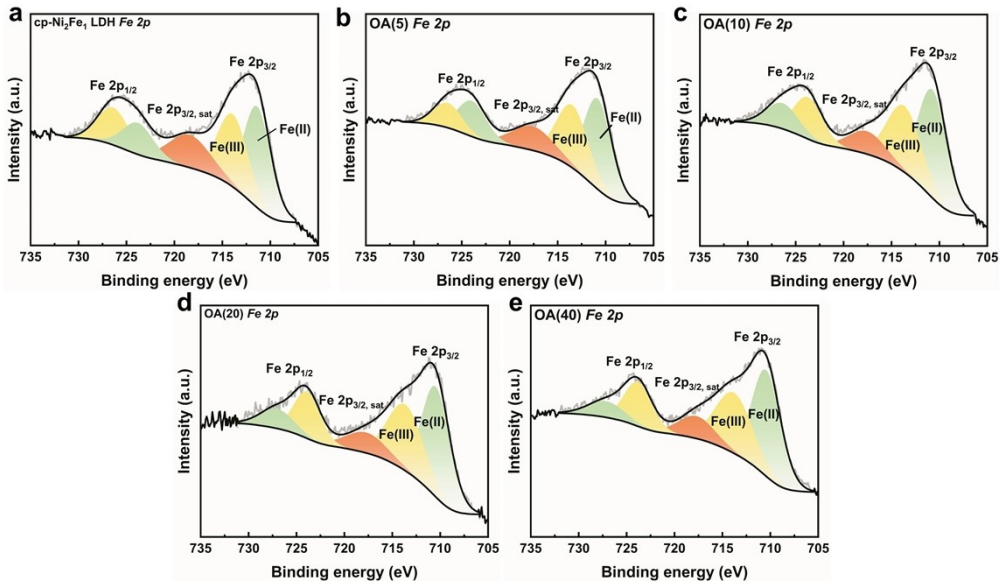

Figure S3. Fe 2p XPS peak fitting of cp-Ni_2Fe_1 LDH and cp-OA(n) NiFe LDH(n= 5, 10, 20, 40).

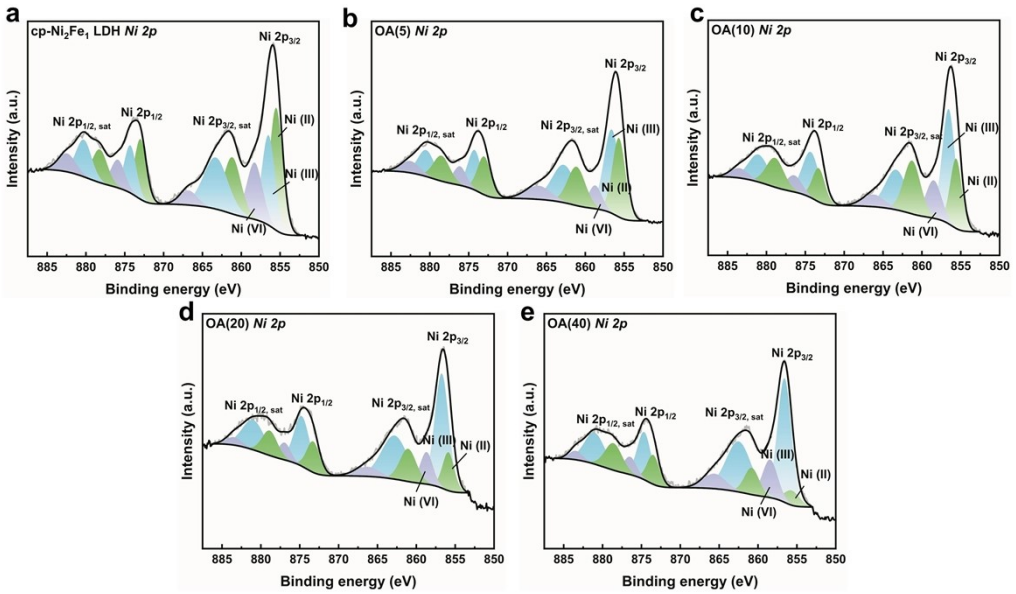

Figure S4. Ni 2p XPS peak fitting of cp-Ni_2Fe_1 LDH and cp-OA(n) NiFe LDH(n= 5, 10, 20, 40).

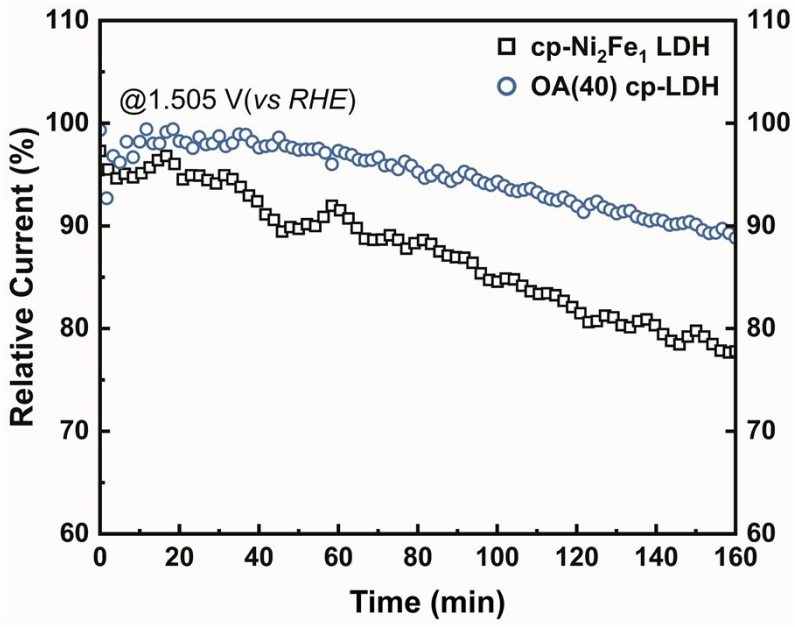

Figure S5. The chronoamperometry tests of cp-Ni_2Fe_1 LDH and OA(40) cp-LDH at 1.505 V vs RHE.

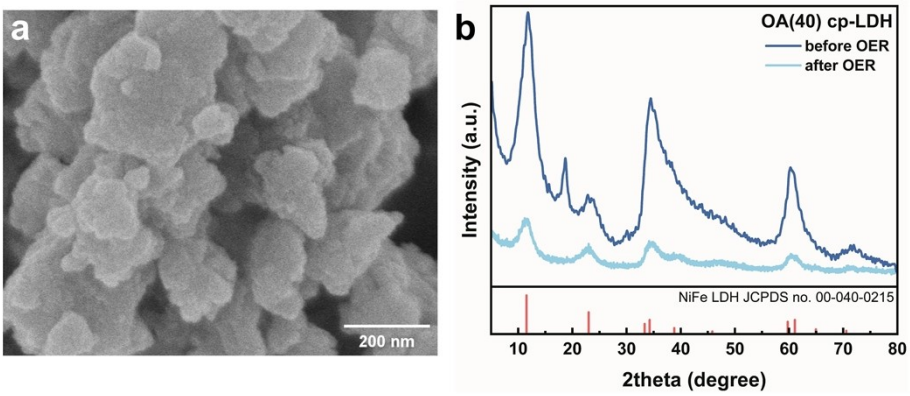

Figure S6. (a) SEM image of cp-OA(40) LDH and (b) XRD pattern of cp-OA(40) LDH before and after OER.

Under the oxygen atmosphere, the BTC of MIL-100 is completely burned to CO_2 and H_2O, and the residual component is Fe_2O_3, according to the proportion calculation:

$$m_{(Fe\%wt)} = m_{vestiges} \times \frac{112}{156},$$

the content of Fe in each portion of MIL-100(Fe) is 11.6%, and BTC is 69.3%. So, 1 g of MIL-100(Fe) powder contains 2.07 mmol of Fe.

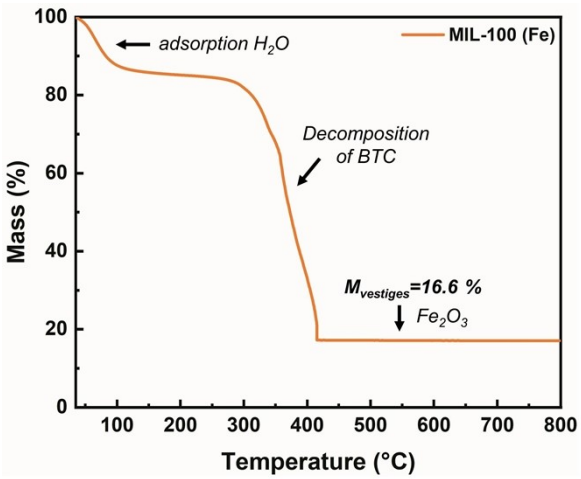

Figure S7. Thermogravimetry analysis of MIL-100(Fe)

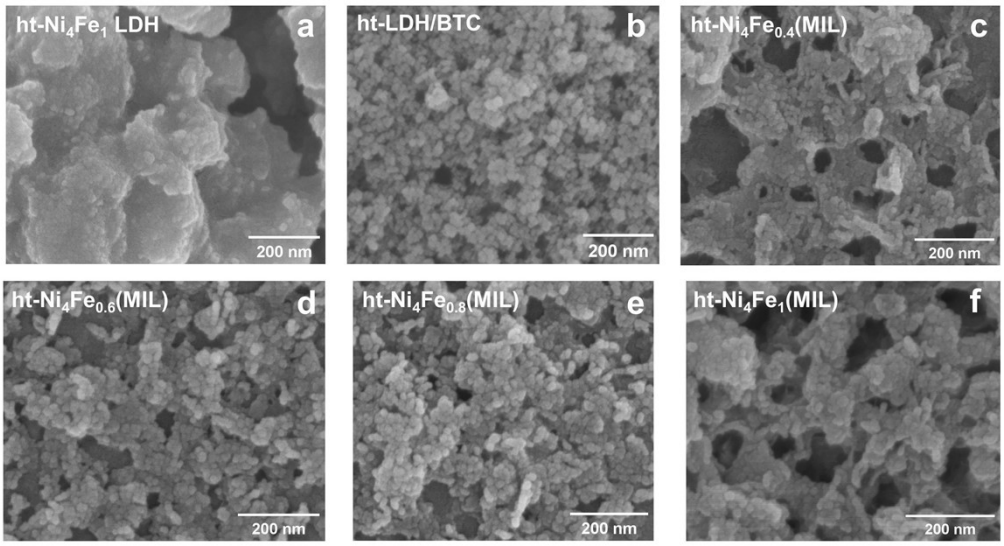

Figure S8. SEM images of (a)ht-Ni_4Fe_1 LDH, (b) ht-LDH/BTC, (c) ht-$Ni_4Fe_{0.4}$(MIL) (d) ht-$Ni_4Fe_{0.6}$(MIL), (e) ht-$Ni_4Fe_{0.8}$(MIL) and (e) ht-Ni_4Fe_1(MIL).

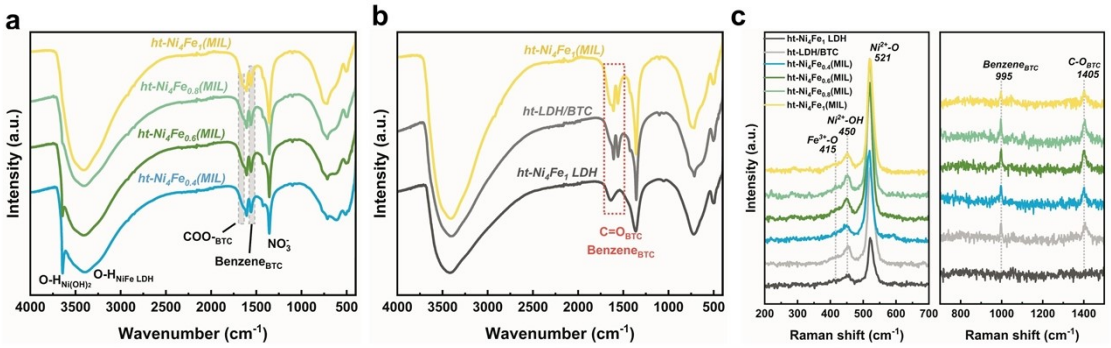

Figure S9. (a),(b) FTIR and (c) Raman spectra of ht-Ni_4Fe_n(MIL) (n= 0.4, 0.6, 0.8, 1), ht-Ni_4Fe_1 LDH and ht-LDH/BTC.

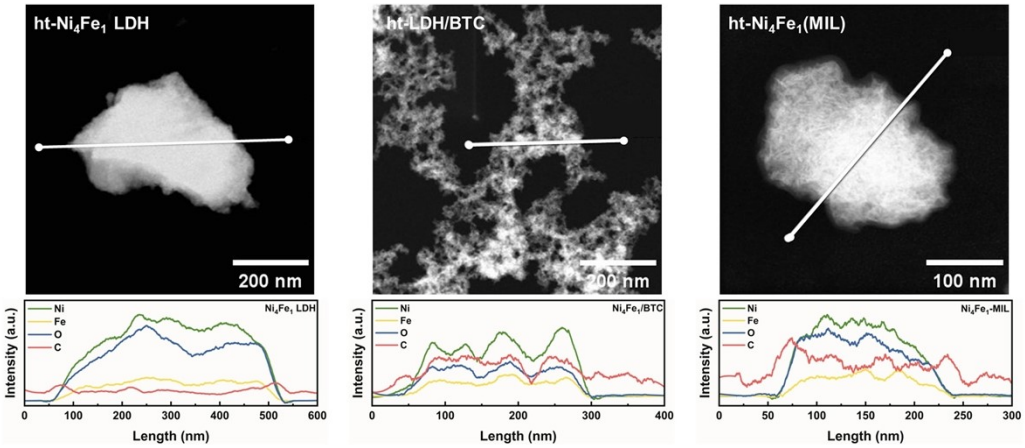

Figure S10. HRTEM EDS line-scanning ht-Ni_4Fe_1(MIL), ht-Ni_4Fe_1 LDH and ht-LDH/BTC.

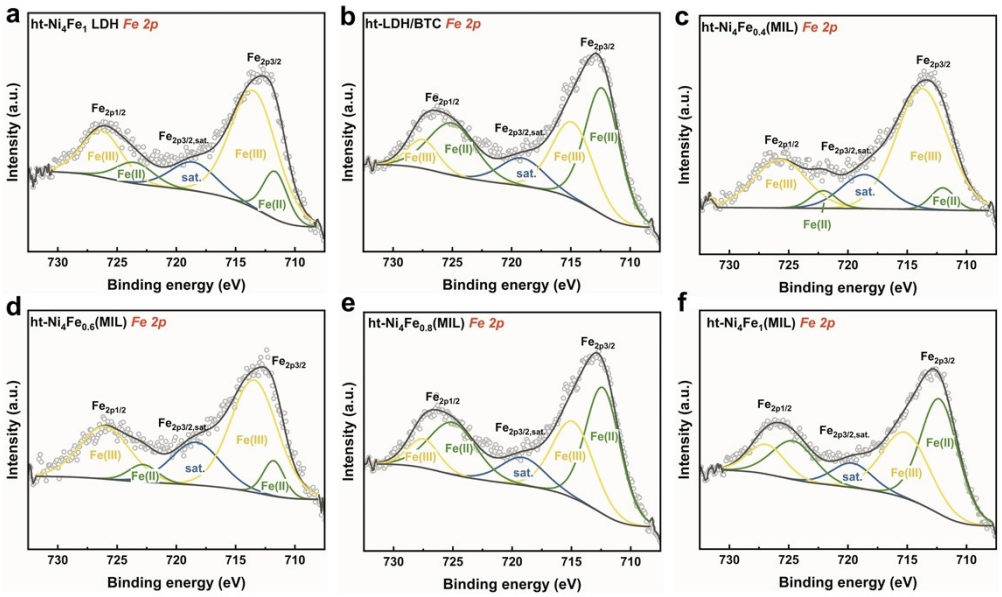

Figure S11. Fe 2p XPS peak fitting of ht-Ni_4Fe_n(MIL) (n= 0.4, 0.6, 0.8, 1), ht-Ni_4Fe_1 LDH and ht-LDH/BTC.

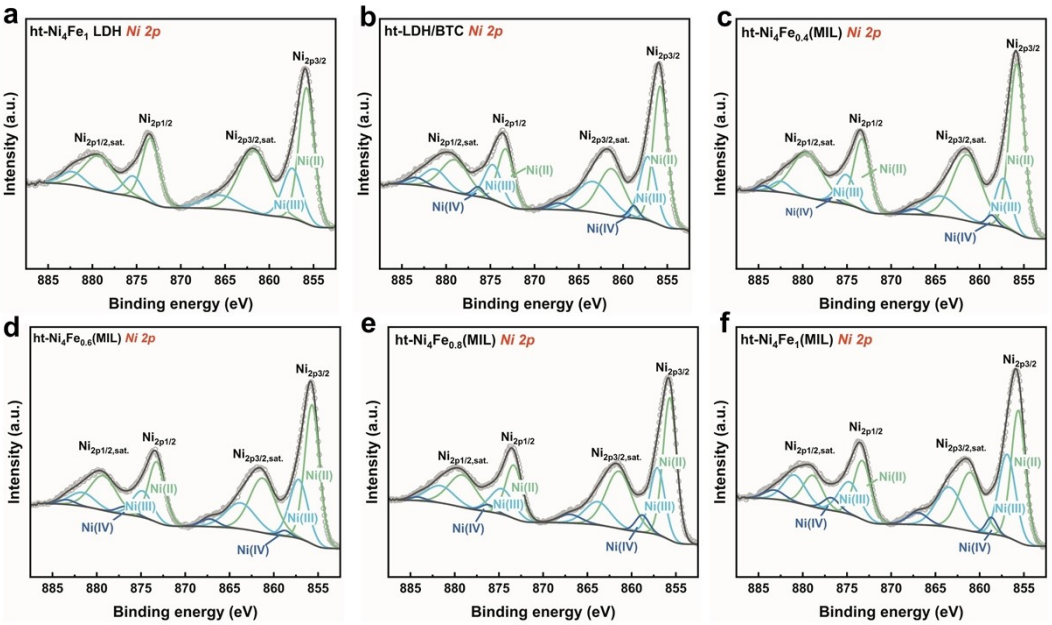

Figure S12. Ni 2p XPS peak fitting of ht-Ni_4Fe_n(MIL) (n= 0.4, 0.6, 0.8, 1), ht-Ni_4Fe_1 LDH and ht-LDH/BTC.

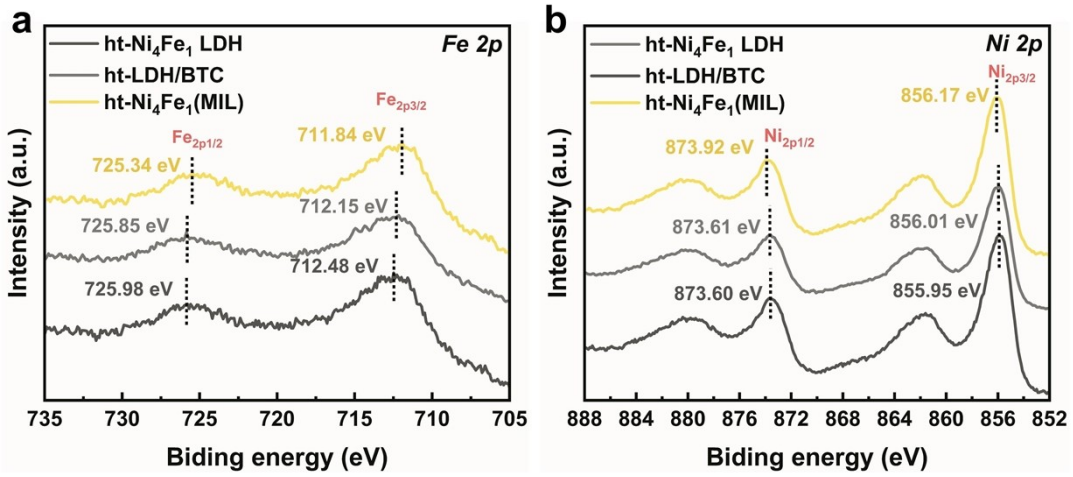

Figure S13. (a) Fe 2p and (d) Ni 2p fine XPS spectra ht-Ni_4Fe_1(MIL), ht-Ni_4Fe_1 LDH and ht-LDH/BTC.

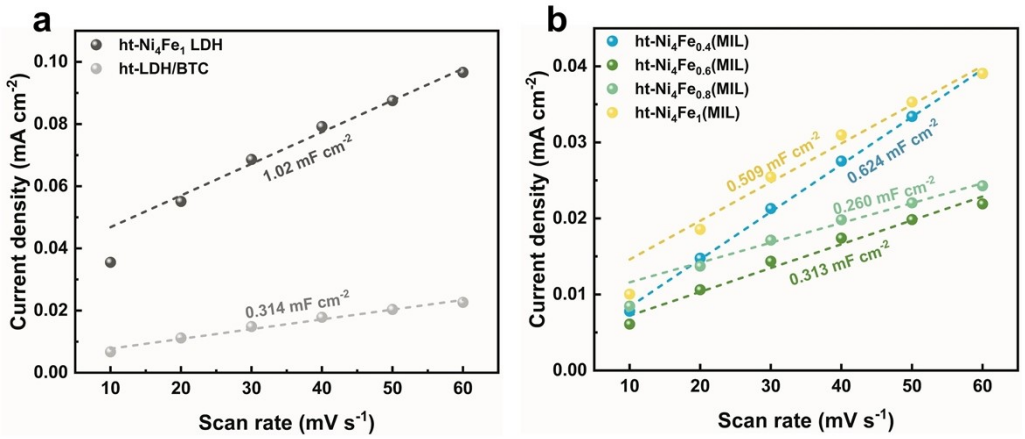

Figure S14. Double layer capacitances of (a) ht-Ni_4Fe_1 LDH, ht-LDH/BTC and (b) ht-Ni_4Fe_n(MIL) (n= 0.4, 0.6, 0.8, 1) estimated by CV at various scan rates.

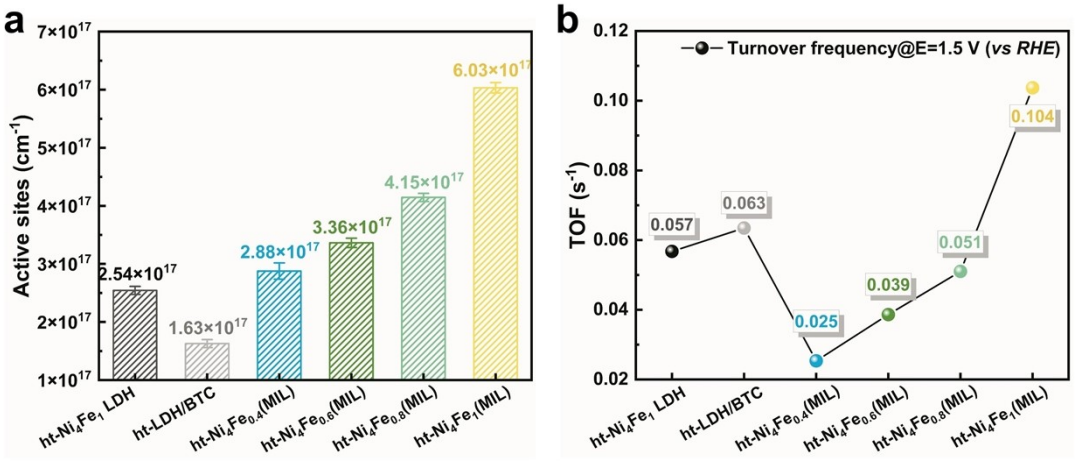

Figure S15. (a) Actives sites of prepared catalyst electrodes and (b) Turnover frequency at 1.5 V (vs RHE).

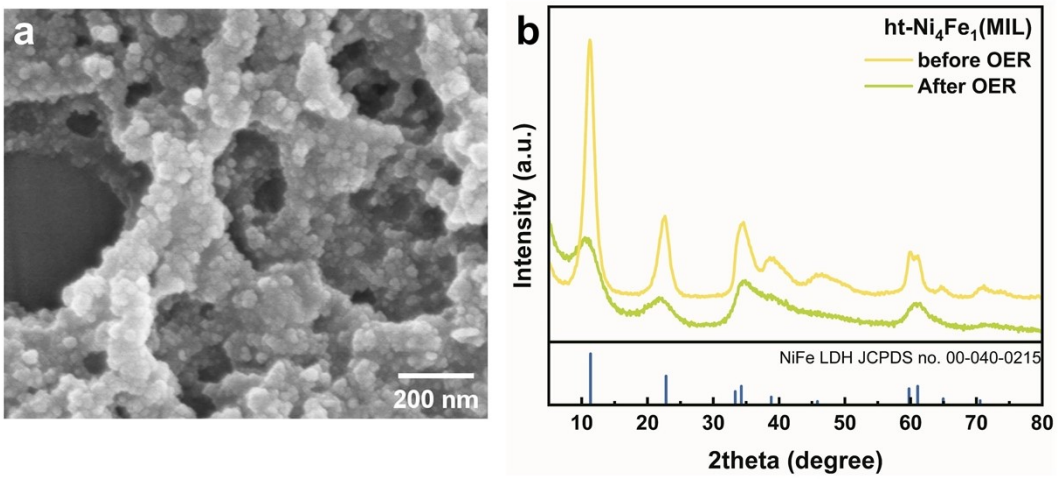

Figure S16. (a) SEM image of ht-Ni_4Fe_1(MIL) and (b) XRD pattern of ht-Ni_4Fe_1(MIL) before and after OER.

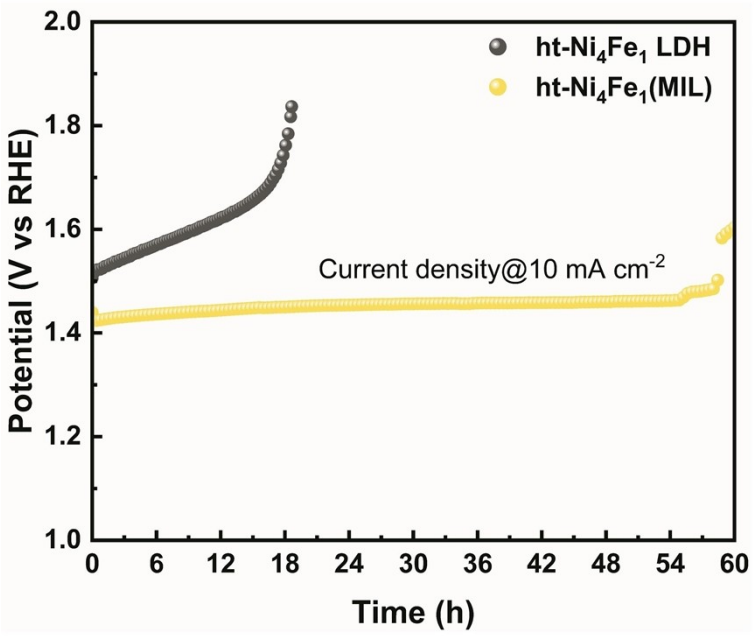

Figure S17. Chronopotentiometry of ht-Ni_4Fe_1 LDH and ht-Ni_4Fe_1(MIL).

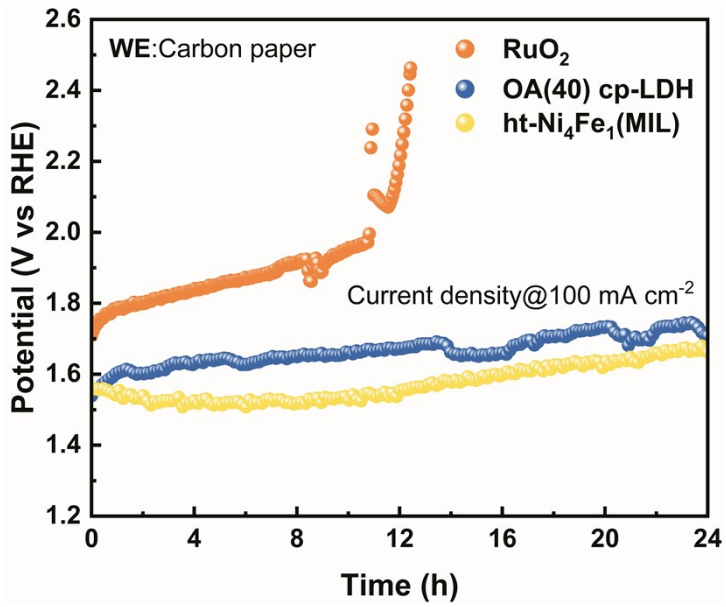

Figure S18. Chronopotentiometry at 100 mA cm^{-2} of RuO_2, cp-OA(40) LDH and ht-Ni_4Fe_1(MIL).